Global membrane tension is independent of polyacrylamide substrate stiffness

Eva Kreysing[1,*], Jeffrey Mc Hugh[2,3,*], Sarah K. Foster[1,4], Kurt Andresen[5], Ryan D. Greenhalgh[1], Eva K. Pillai[1], Andrea Dimitracopoulos[1], Ulrich F. Keyser[2,#], Kristian Franze[1,6,7,#]

1) Department of Physiology, Development and Neuroscience, University of Cambridge, Cambridge CB2 3DY, UK

2) Biological and Soft Systems, Maxwell Centre, Cavendish Laboratory, Cambridge CB3 0HE, UK

3) Neuroglial Interactions in Cerebral Physiopathology, CIRB, CNRS UMR 7241/INSERM U1050, Collège de France, Paris 75005, France

4) Systems Biology of Microbial Communities, Cluster of Excellence – CMFI, University of Tübingen, 72076 Tübingen, Germany

5) Department of Physics, Gettysburg College, Gettysburg, PA 17325, United States of America

6) Institute of Medical Physics, Friedrich-Alexander-Universität Erlangen-Nürnberg, 91052 Erlangen, Germany.

7) Max-Planck-Zentrum für Physik und Medizin, 91054 Erlangen, Germany

* These authors contributed equally.

\# To whom correspondence should be addressed: ufk20@cam.ac.uk or kf284@cam.ac.uk

Abstract

Most animal cells are surrounded by a cell membrane and an underlying actomyosin cortex. Both structures are linked, and they are under tension. In-plane membrane tension and cortical tension both influence many cellular processes, including cell migration, division, and endocytosis. However, while actomyosin tension is regulated by substrate stiffness, how membrane tension responds to mechanical substrate properties is currently poorly understood. Here, we probed the effective membrane tension of neurons and fibroblasts cultured on glass and polyacrylamide substrates of varying stiffness using optical tweezers. In contrast to actomyosin-based traction forces, both peak forces and steady state tether forces of cells cultured on hydrogels were independent of substrate stiffness and did not change after blocking myosin II activity using blebbistatin, indicating that tether and traction forces are not directly linked. Peak forces in fibroblasts on hydrogels were about twice as high as those in neurons, indicating stronger membrane-cortex adhesion in fibroblasts. Steady state tether forces were generally higher in cells cultured on hydrogels than on glass, which we explain by a mechanical model. Our results provide new insights into the complex regulation of effective membrane tension and pave the way for a deeper understanding of the biological processes it instructs.

38 ## Introduction

39 The cell membrane is supported by the underlying actomyosin cortex, and molecular linkers
40 form tight connections between the two layers. Osmotic pressure resulting from ion gradients
41 across the membrane and interactions of the membrane with the force-generating actomyosin
42 cytoskeleton contribute to a tension across the membrane. This membrane tension regulates
43 many cellular processes, such as cell migration, division, stem cell fate choice, and endo- and
44 exocytosis[1–6]. Despite its biological importance[7–9], membrane tension is still difficult to
45 quantify. In-plane membrane tension is defined as the force per unit length acting tangentially
46 on the plasma membrane. Because of the membrane's coupling to cytoskeletal elements,
47 measurements of the 'effective' membrane tension usually contain contributions of the
48 underlying actomyosin cortex and other force-generating elements[10,11].

49 The actomyosin cortex is coupled to the extracellular environment through membrane proteins
50 such as integrins and cadherins. It generates tensile forces which are exerted on the
51 environment. These forces, and hence cytoskeletal tension, increase with substrate stiffness
52 for most cell types[12,13], suggesting that the measured effective membrane tension should also
53 increase on stiffer substrates. However, the regulation of membrane tension by substrate
54 mechanics is yet to be probed experimentally.

55

56 ## Results

57 Here, we used optical tweezers (OT) to probe membrane properties of cells cultured on
58 polyacrylamide substrates of different stiffnesses as well as on glass. Using a membrane-

59 adherent bead held in an optical trap, we pulled membrane tethers from cells, and the resulting
60 tether forces served as an indicator for effective membrane tension [2,14,15] (Fig. 1a, b; Fig. S1,
61 Video S1). Throughout a pull, the force on the tether can be continuously monitored, resulting
62 in a characteristic force-time curve (Fig. 1c). The force rises quickly after initiation of the pull
63 and reaches a peak before decreasing sharply. In agreement with Sheetz[14], we attribute this
64 peak force (PF) to the initial local detachment of plasma membrane from the actomyosin cortex
65 (Fig. 1a).

66 Subsequently, the tether is pulled until it reaches a set length. During this elongation process,
67 the plasma membrane slides over the actin cortex while bonds between the membrane and the
68 lipid-binding proteins located in or at the cortex are broken and quickly re-established[16].
69 Following the elongation phase, the bead is held in a stable position and the steady-state force
70 (SSF) is measured (Fig. 1b). The SSF is thought to reflect a combination of the in-plane plasma
71 membrane tension and the cortical tension, with the strength of the membrane-cortex
72 adhesion determining the coupling between these two elements[16,17].

73 To test the effect of substrate mechanics and cortical tension on effective membrane tension,
74 we performed tether pulls in fibroblasts, which possess a dense actomyosin cortex, and in
75 neuronal axons, whose sub-membranous cytoskeleton is characterized by actin rings spaced by
76 spectrin tetramers[18]. Cells were cultured on glass as well as on hydrogels fabricated within a
77 stiffness range adjusted to match their natural environment. For fibroblasts, hydrogel
78 stiffnesses ranged from 100Pa (very soft; similar to subcutaneous adipose tissue), to 10kPa
79 (stiff; already in the stiffness range of many fibrotic tissues)[19]. For neurons, the highest

80 substrate stiffness used was 1kPa, corresponding to the highest stiffness experienced by this
81 type of neuron *in vivo*[20].

82 Peak forces (PFs) measured in fibroblasts were about twice as high as those measured in
83 neuronal axons (Fig. 2b, f). Within each cell type, PFs were similar across all tested hydrogel
84 substrates. Steady state forces (SSFs), which were comparable between fibroblasts and
85 neurons, were also similar across all polyacrylamide substrate stiffnesses (Fig. 2c, g).

86 In contrast, actomyosin-based traction forces are known to scale with substrate stiffnesses for
87 both neurons and fibroblasts[21,22]. We explicitly measured traction forces in our culture
88 conditions and confirmed that traction forces exhibited by both cell types increased
89 significantly with increasing substrate stiffness within the investigated stiffness range (Fig. 2d,
90 Fig. S3). Similarly, net forces, which are obtained by integrating traction forces across neuronal
91 growth cones, and which provide an approximation for the tension exerted by a growth cone
92 on its axon[21,23], significantly increased on stiffer substrates (Fig 2h). These data indicated that
93 traction forces and net forces assessed by 2D traction force microscopy and tether forces
94 measured by OT are not tightly coupled.

95 Cellular cortical tension is mediated by actomyosin contractility[24]. However, cortical tension
96 further away from adhesion sites, where traction forces are generated and transmitted to the
97 environment, was recently suggested to be largely independent of traction forces[22]. In order to
98 further examine the interplay between cortical tension and effective membrane tension, we
99 measured tether forces in fibroblasts cultured on 10 kPa hydrogels, where we would expect the
100 highest cytoskeletal tension[22], following treatment with the myosin II (and thus contractility)

101 inhibitor blebbistatin. Blebbistatin treatment had no significant effect on either PFs or SSFs (Fig.
102 3), suggesting that there is indeed no strong coupling between actomyosin-based cortical
103 tension and global effective membrane tension in cells cultured on hydrogels.

104 As numerous *in vitro* studies use glass-bottomed culture dishes, and the surface properties of
105 glass differ considerably from those of hydrogels, we also cultured fibroblasts and neurons on
106 glass to test whether effective membrane tension is comparable in both culture environments.

107 In neurons, PFs measured in axons cultured on glass were indeed like those observed on
108 hydrogels (Fig. 2f). However, PFs for fibroblasts cultured on glass were significantly lower than
109 those for fibroblasts grown on hydrogels (Fig. 2b). Similarly, SSFs were significantly lower for
110 fibroblasts and neurons cultured on glass compared to those cultured on hydrogels (Fig. 2c, g).
111 Unlike on hydrogels, tether forces measured on glass were similar for fibroblasts and neurons
112 (Fig. 2).

113 While PFs did not change significantly after blocking actomyosin contractility in fibroblasts
114 cultured on glass, SSFs increased on glass following blebbistatin treatment[25] (Fig 3b), reaching
115 values similar to SSFs seen in fibroblasts cultured on hydrogels. These data showed that
116 effective membrane tension depends on the type of culture substrate, and they suggested that
117 the coupling between the cell cortex and the membrane also differs between glass and
118 hydrogel substrates.

119

120 **Discussion**

121 Here we found that the steady-state tether forces, which are thought to scale with effective
122 membrane tension, do not change as a function of hydrogel substrate stiffness within a
123 physiologically relevant stiffness range in both fibroblasts and neurons (Fig. 2c, g). In contrast,
124 actomyosin-based traction and net forces increased on stiffer substrates (Fig. 2d, h), as shown
125 previously[22], suggesting that the effective membrane tension measured by OT is not directly
126 linked to cellular contractility on hydrogels[26]. In line with this interpretation, the application of
127 the myosin II blocker, blebbistatin, did not alter the effective membrane tension of fibroblasts
128 cultured on hydrogels (Fig. 3). Alternatively, membrane tension might be influenced by cortical
129 tension on short time scales but is then actively regulated to resume original values quickly[27].

130 Another possibility is that traction forces transmitted from focal adhesions to the cortex might
131 dissipate within a finite distance, so that overall cortical tension would not scale with local
132 traction forces[22]. If cortical and membrane tension are coupled, membrane tension would only
133 increase locally[28] near focal adhesions, which would not be seen when probed further away.
134 Such local membrane tension fluctuations would explain, for example, why the
135 mechanosensitive ion channel Piezo1, which is thought to be activated by membrane tension, is
136 activated only near focal adhesion sites despite being distributed across the whole cell
137 surface[29].

138 The effective membrane tension was higher in cells cultured on hydrogels than in those
139 cultured on glass (Fig. 2). Fibroblasts developed much stronger stress fibres on glass than on
140 hydrogels (Fig. S2)[30]. The strong contraction of stress fibres on glass might deform the cortex
141 between focal adhesions, this way releasing cortical tension and causing the membrane to
142 relax, as schematically indicated in Figure 4. This could not only explain why SSFs in fibroblasts

143 were lower on glass than on hydrogels (Fig. 2c, Fig. 4b) but also why blebbistatin treatment,
144 which relaxes stress fibres, led to a significant increase in SSFs on glass but not on hydrogels
145 (Figs. 3b, 4c-d). This hypothesis agrees with recent experiments showing that perturbations of
146 stress fibres lead to an increase in tension in the nearby actin cortex[31]. The tension exerted by
147 growth cones on the distal axon, which increased on stiffer substrates (Fig. 2h), could similarly
148 lead to membrane relaxation in neurons cultured on glass (Fig. 2g). Alternatively, or
149 additionally, differences in physical and chemical properties between glass and hydrogels could
150 also activate different signalling pathways involved in the regulation of membrane tension
151 homeostasis[27].

152 The PF, which is the initial force required to detach the membrane from the cortex, is related to
153 membrane-cortex adhesion[14] (in analogy to attempting to open Velcro from the middle).
154 Fibroblasts have a dense actomyosin cortex, and proteins such as ezrin/radixin/moesin (ERM)
155 can link the membrane to the cortex across the cell surface. Neuronal axons, on the other hand,
156 have a periodic actin-spectrin network underneath their membrane[18] and much less area for
157 ERM proteins to connect the membrane to actin rings. This morphological difference may lead
158 to lower membrane-cortex adhesion in axons compared to fibroblasts, explaining why PFs are
159 about twice as high in fibroblasts compared to axons cultured on physiologically stiff hydrogels.
160 A low membrane-cortex coupling could also explain why tethers pulled from axons can freely
161 "slide" along the axon as observed in a previous[15] and the current study (video S2). To our
162 knowledge, tether sliding has not been reported in fibroblasts.

163 Our results confirm that membrane tension measurements need to be interpreted carefully.
164 Effective membrane tension did not depend on substrate stiffness within a physiological

165 stiffness range, yet it varies between hydrogels and glass, and between cell types. Future
166 technological developments enabling highly resolved quantitative membrane tension
167 measurements will shed light on the molecular control of local membrane tension, an
168 important regulator of many cellular functions.

Acknowledgments

The authors would like to thank Alex Winkel and Joy Thompson for AFM measurements of hydrogels, Liz Williams for preparation of hydrogels, and Ewa Paluch, Ruby Peters and Aki Stubb for discussions. J. Mc H. acknowledges funding from AFOSR (Grant No. FA9550-17-1-0118). S. K. F. acknowledges funding from the Herchel Smith Foundation. U. F. K. was supported by an ERC Consolidator Grant DesignerPores No. 647144, K. F. was supported by the European Research Council (Consolidator Grant 772426) and the Alexander von Humboldt Foundation (Alexander von Humboldt Professorship).

Author Contributions

J. Mc H., E. K., and K. A. performed tether pulling experiments. J. Mc H. analysed the results from OT experiments. E. K. cultured 3T3 fibroblasts and prepared hydrogels. S. K. F. dissected and cultured Xenopus laevis RGCs and prepared hydrogels. A.D. performed TFM experiments with 3T3 fibroblasts. R. G. performed the TFM experiments with neurons and all TFM analyses. E. K. and E. P. performed the immunostainings. J. Mc H., E. K., K. F., and U. F. K. designed experiments with 3T3 fibroblasts. J. Mc H., S. K. F., K. A., and U. F. K. designed pulling experiments with X. laevis RGCs. S. K. F., Mc H., E. K., U.F.K. and K. F. conceived the project. E. K., J. Mc H., S. K. F., U.F.K. and K.F. wrote the manuscript.

Competing interests

The authors declare no competing interests.

189 **References**

190 1. Raucher, D. & Sheetz, M. P. Cell Spreading and Lamellipodial Extension Rate Is Regulated by
191 Membrane Tension. *J. Cell Biol.* **148**, 127–136 (2000).
192 2. Nussenzveig, H. M. Cell membrane biophysics with optical tweezers. *Eur. Biophys. J.* **47**, 499–
193 514 (2018).
194 3. Gauthier, N. C., Fardin, M. A., Roca-Cusachs, P. & Sheetz, M. P. Temporary increase in plasma
195 membrane tension coordinates the activation of exocytosis and contraction during cell
196 spreading. *Proc. Natl. Acad. Sci. U. S. A.* **108**, 14467–14472 (2011).
197 4. Keren, K. *et al.* Mechanism of shape determination in motile cells. *Nature* **453**, 475–480
198 (2008).
199 5. De Belly, H. *et al.* Membrane Tension Gates ERK-Mediated Regulation of Pluripotent Cell Fate.
200 *Cell Stem Cell* **28**, 273-284.e6 (2021).
201 6. Dai, J. & Sheetz, M. P. Regulation of endocytosis, exocytosis, and shape by membrane tension.
202 *Cold Spring Harb. Symp. Quant. Biol.* **60**, 567–571 (1995).
203 7. Sheetz, M. P. Cell control by membrane–cytoskeleton adhesion. *Nat. Rev. Mol. Cell Biol.* **2**,
204 392–396 (2001).
205 8. Pontes, B., Monzo, P. & Gauthier, N. C. Membrane tension: A challenging but universal
206 physical parameter in cell biology. *Semin. Cell Dev. Biol.* **71**, 30–41 (2017).
207 9. Pontes, B. *et al.* Membrane tension controls adhesion positioning at the leading edge of cells.
208 *J. Cell Biol.* **216**, 2959–2977 (2017).
209 10. Salbreux, G., Charras, G. & Paluch, E. Actin cortex mechanics and cellular morphogenesis.
210 *Trends Cell Biol.* **22**, 536–545 (2012).

211 11. Clark, A. G., Wartlick, O., Salbreux, G. & Paluch, E. K. Stresses at the Cell Surface during
212 Animal Cell Morphogenesis. *Curr. Biol.* **24**, R484–R494 (2014).
213 12. Califano, J. P. & Reinhart-King, C. A. Substrate Stiffness and Cell Area Predict Cellular
214 Traction Stresses in Single Cells and Cells in Contact. *Cell. Mol. Bioeng.* **3**, 68–75 (2010).
215 13. Sabass, B., Gardel, M. L., Waterman, C. M. & Schwarz, U. S. High Resolution Traction
216 Force Microscopy Based on Experimental and Computational Advances. *Biophys. J.* **94**, 207–
217 220 (2008).
218 14. Sheetz, M. P. Cell control by membrane–cytoskeleton adhesion. *Nat. Rev. Mol. Cell Biol.*
219 **2**, 392–396 (2001).
220 15. Datar, A., Bornschlögl, T., Bassereau, P., Prost, J. & Pullarkat, P. A. Dynamics of membrane
221 tethers reveal novel aspects of cytoskeleton-membrane interactions in axons. *Biophys. J.* **108**,
222 489–497 (2015).
223 16. Sens, P. & Plastino, J. Membrane tension and cytoskeleton organization in cell motility. *J.*
224 *Phys. Condens. Matter* **27**, (2015).
225 17. Gauthier, N. C., Masters, T. A. & Sheetz, M. P. Mechanical feedback between membrane
226 tension and dynamics. *Trends Cell Biol.* **22**, 527–535 (2012).
227 18. Xu, K., Zhong, G. & Zhuang, X. Actin, spectrin, and associated proteins form a periodic
228 cytoskeletal structure in axons. *Science* **339**, 452–456 (2013).
229 19. Wells, R. G. Tissue Mechanics and Fibrosis. *Biochim. Biophys. Acta* **1832**, 884–890 (2013).
230 20. Franze, K., Janmey, P. A. & Guck, J. Mechanics in Neuronal Development and Repair.
231 *Annu. Rev. Biomed. Eng.* **15**, 227–251 (2013).

232 21. Koch, D., Rosoff, W. J., Jiang, J., Geller, H. M. & Urbach, J. S. Strength in the Periphery:
233 Growth Cone Biomechanics and Substrate Rigidity Response in Peripheral and Central
234 Nervous System Neurons. *Biophys. J.* **102**, 452–460 (2012).
235 22. Rheinlaender, J. *et al.* Cortical cell stiffness is independent of substrate mechanics. *Nat.*
236 *Mater.* **19**, 1019–1025 (2020).
237 23. Franze, K. Integrating Chemistry and Mechanics: The Forces Driving Axon Growth. *Annu.*
238 *Rev. Cell Dev. Biol.* **36**, 61–83 (2020).
239 24. Chugh, P. *et al.* Actin cortex architecture regulates cell surface tension. *Nat. Cell Biol.* **19**,
240 689–697 (2017).
241 25. Lieber, A. D., Yehudai-Resheff, S., Barnhart, E. L., Theriot, J. A. & Keren, K. Membrane
242 Tension in Rapidly Moving Cells Is Determined by Cytoskeletal Forces. *Curr. Biol.* **23**, 1409–
243 1417 (2013).
244 26. Mandal, K. *et al.* Soft hyaluronic gel promotes cell spreading, stress fibers, focal adhesion,
245 membrane tension by phosphoinositide signaling, not traction force. *ACS Nano* **13**, 203–214
246 (2019).
247 27. Thottacherry, J. J. *et al.* Mechanochemical feedback control of dynamin independent
248 endocytosis modulates membrane tension in adherent cells. *Nat. Commun.* **9**, 1–14 (2018).
249 28. Shi, Z., Graber, Z. T., Baumgart, T., Stone, H. A. & Cohen, A. E. Cell membranes resist flow.
250 *Cell* **175**, 1769-1779.e13 (2018).
251 29. Ellefsen, K. L. *et al.* Myosin-II mediated traction forces evoke localized Piezo1-dependent
252 Ca 2+ flickers. *Commun. Biol.* **2**, 1–13 (2019).

253 30. Walcott, S. & Sun, S. X. A mechanical model of actin stress fiber formation and substrate
254 elasticity sensing in adherent cells. *Proc. Natl. Acad. Sci.* **107**, 7757–7762 (2010).
255 31. Vignaud, T. *et al.* Stress fibres are embedded in a contractile cortical network. *Nat.*
256 *Mater.* 1–11 (2020) doi:10.1038/s41563-020-00825-z.
257 32. Leung, K.-M. *et al.* Asymmetrical β-actin mRNA translation in growth cones mediates
258 attractive turning to netrin-1. *Nat. Neurosci.* **9**, 1247–1256 (2006).
259 33. Nieuwkoop, P. D. & Faber, J. *Normal table of xenopus laevis (daudin)*. (Routledge, 1994).
260 34. Mc Hugh, J., Andresen, K. & Keyser, U. F. Cation dependent electroosmotic flow in glass
261 nanopores. *Appl. Phys. Lett.* **115**, 113702 (2019).
262 35. Gittes, F. & Schmidt, C. F. Chapter 8 signals and noise in micromechanical measurements.
263 in *Methods in cell biology.* vol. 55 129–156 (Academic Press, 1997).
264 36. Buer, C. S., Weathers, P. J. & Swartzlander, G. A. Changes in Hechtian strands in cold-
265 hardened cells measured by optical microsurgery. *Plant Physiol.* **122**, 1365–1377 (2000).
266 37. Kucik, D. F., Kuo, S. C., Elson, E. L. & Sheetz, M. P. Preferential attachment of membrane
267 glycoproteins to the cytoskeleton at the leading edge of lamella. *J. Cell Biol.* **114**, 1029–1036
268 (1991).
269 38. Hochmuth, R. M., Shao, J. Y., Dai, J. & Sheetz, M. P. Deformation and flow of membrane
270 into tethers extracted from neuronal growth cones. *Biophys. J.* **70**, 358–369 (1996).
271 39. Pontes, B. *et al.* Cell cytoskeleton and tether extraction. *Biophys. J.* **101**, 43–52 (2011).
272 40. Moshayedi, P. *et al.* The relationship between glial cell mechanosensitivity and foreign
273 body reactions in the central nervous system. *Biomaterials* **35**, 3919–3925 (2014).

41. Koser, D. E. *et al.* Mechanosensing is critical for axon growth in the developing brain. *Nat. Neurosci.* **19**, 1592–1598 (2016).

42. Moshayedi, P. *et al.* Mechanosensitivity of astrocytes on optimized polyacrylamide gels analyzed by quantitative morphometry. *J. Phys. Condens. Matter* **22**, (2010).

Figures

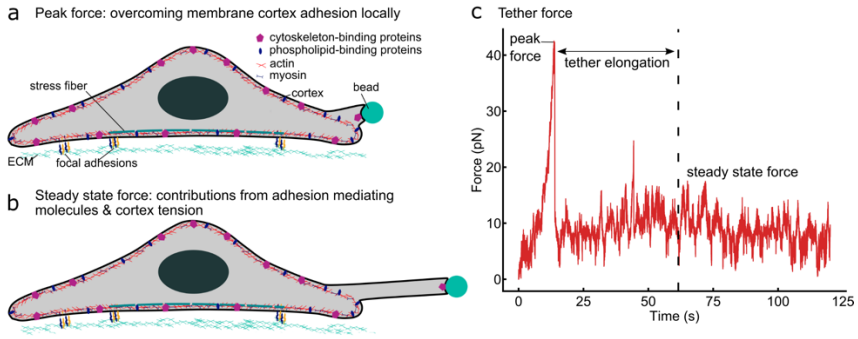

Figure 1: Illustration of an OT measurement. Peak and steady state tether forces provide different insights into cell membrane properties. (a) When an OT pull is initiated, the local membrane-cortex adhesion first needs to be overcome, resulting in a peak force (PF) measured at the beginning of the experiment (see (c)). (b) After tether extension, the bead is held stationary, and the steady state force (SSF), which scales with effective membrane tension, is recorded. (c) A typical force-time curve recorded during a tether pull, showing a peak (PF) at the beginning of the pull and a plateau (SSF) when the tether is held at its maximum extension.

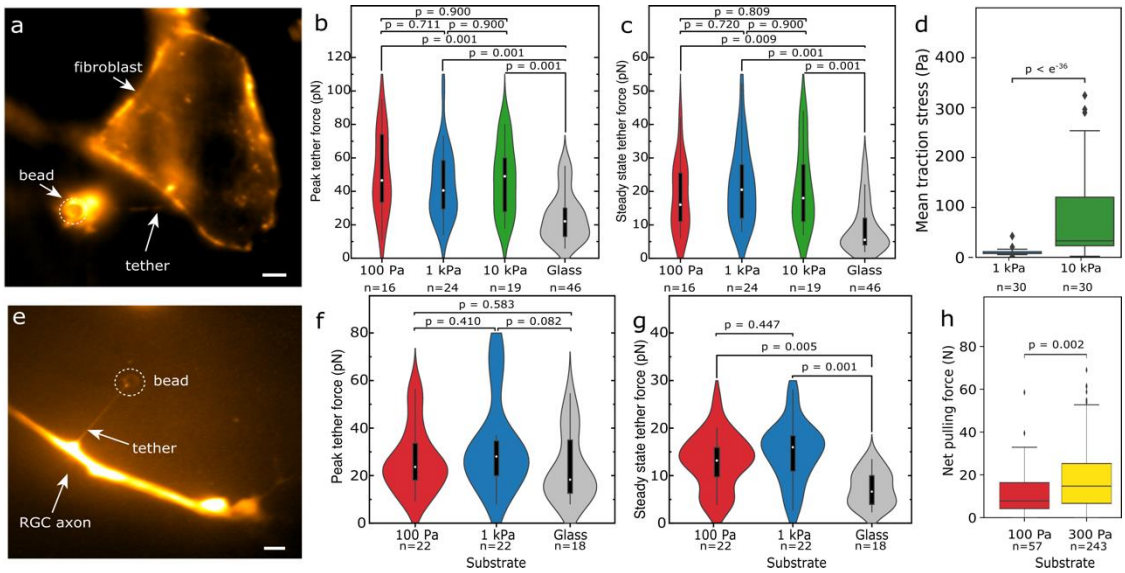

Figure 2: Tether and traction forces of fibroblasts and neurons on different substrates. (a-d) 3T3 fibroblasts and (e-h) *Xenopus* retinal ganglion cell axons; shear moduli of polyacrylamide substrates are provided in Pa. (a, e) Fluorescence images of membrane tethers pulled from a 3T3 fibroblast and an axon. Fibroblast membranes were labelled with CellMask membrane stain, neurons with Tetramethylrhodamine Dextran. Scale bars: 5µm. (b) Peak tether forces (PFs) and (c) steady state tether forces (SSFs) were similar on all hydrogels irrespective of their stiffness (Kruskal-Wallis tests followed by Tukey posthoc tests), but significantly larger than on glass. (d) 3T3 fibroblasts exerted higher traction forces on stiffer hydrogels compared to on softer ones (two-tailed Mann-Whitney test). (f) PFs in axons were similar on all hydrogel and glass substrates. (g) SSFs in neurons were similar on different hydrogels but higher than those measured on glass. (h) Net forces (growth cone forces pulling on the axon) were higher on stiffer hydrogels than on softer ones (two-tailed Mann-Whitney test).

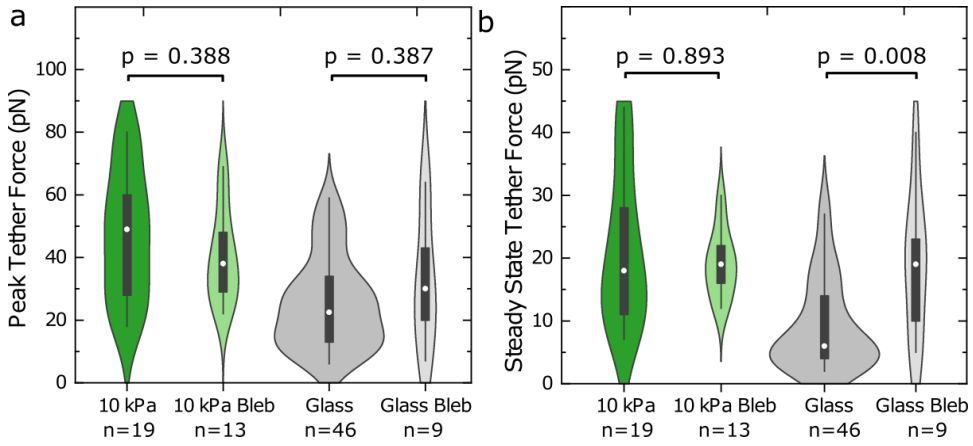

Figure 3: Inhibition of actomyosin contractility increases SSFs on glass but not on hydrogels. (a) The application of 20 µM Blebbistatin did not significantly alter PFs on hydrogels or on glass (Mann-Whitney test). (b) SSFs of fibroblasts grown on glass but not on hydrogels increased significantly following blebbistatin treatment. The untreated conditions correspond to the data shown in Figure 2.

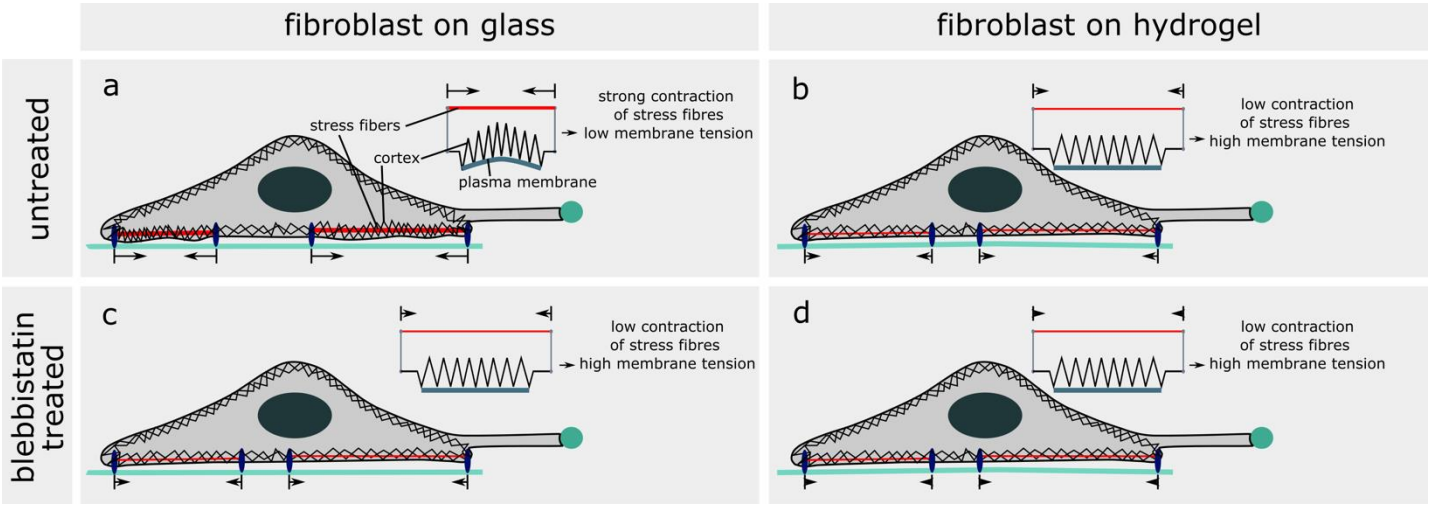

Figure 4: Toy model of substrate type-dependent effective membrane tension. Schematic representation of the cell cortex and stress fibres in fibroblasts on glass and hydrogel substrates without and with blebbistatin treatment. (a) In fibroblasts on glass substrates without blebbistatin treatment, the strong contraction of stress fibres might relax the tension in the cortex and thus reduce membrane tension. (b) In fibroblasts on hydrogel substrates without blebbistatin treatment, we observe fewer stress fibres, most likely resulting in lower contractility and less relaxation of the membrane. The resulting membrane tension is higher compared to that of cells on glass. (c) In fibroblasts on glass substrates with blebbistatin treatment, the stress fibres relax. This might increase membrane tension. (d) In fibroblasts on hydrogel substrates with blebbistatin treatment, fewer stress fibres relax, and the effect on membrane tension is too low to be detected by OT.

322 ## Materials and methods

323 ### NIH 3T3 fibroblast cell culture

324 3T3 cells were cultured in plastic cell culture flasks in culture media (90 ml DMEM with glutamine
325 (Gibco 22320-022), 10 ml Fetal Bovine Serum (Gibco 25300054), 1 ml Penicillin-Streptomycin-
326 Amphotericin B Mixture (PSF, Lonza 17-745E)). After reaching confluency, cells were
327 enzymatically detached. For this step, cells were washed twice with prewarmed (37°C) PBS
328 (Sigma D8537) and then incubated with 1ml 10% TrypLE (Thermo Fisher Scientific A1285901) in
329 PBS at 37°C for 5 min. 5 ml culture media was then added, and the cells were cultured in fresh
330 culture flasks or plated on glass dishes and polyacrylamide (PAA) hydrogels for 4-48 h prior to
331 experiments.

332 Hydrogels of 3 different elastic moduli (shear moduli = 100 Pa,1 kPa, and 10 kPa) were prepared
333 and functionalized as described below. PAA gels as well as glass bottom culture dishes were
334 coated with 0.01 mg/ml PDL in PBS for at least 4 h (typically overnight) followed by 0.02 mg/ml
335 fibronectin in PBS for at least 4 h. Culture media was exchanged with prewarmed (37°C) imaging
336 media (Live Cell Imaging Solution, henceforth 'imaging media' (Thermo Fisher Scientific
337 A14291DJ)) supplemented with 1% PSF 15 min prior to measurements.

338 For the blebbistatin treatment, cells were incubated with 20 µM blebbistatin (Sigma-Aldrich,
339 B0560-1MG) for 15 min prior to measurement. For visualisation of membrane tethers,
340 fibroblasts were stained with CellMask Orange Plasma Membrane Stain (ThermoFisher Scientific,
341 USA, C10045-100 µl). The dye was added to the imaging media in the culture dish at 1:1000
342 dilution 15 min prior to the tether pulls.

343 *Xenopus laevis* retinal ganglion cell culture

344 All animal experiments were conducted in compliance with the Ethical Review Committee of the
345 University of Cambridge and Home office Guidelines.

346 *Xenopus* embryos were derived from *in vitro* fertilization of eggs kindly provided by the Gurden
347 Institute Frog Facility (University of Cambridge, UK). For fluorescent labelling of *Xenopus*
348 neurons, 5 nL of 0.2% w/v tetramethylrhodamine-labeled dextran (Thermo Fisher, D3308)
349 diluted in nuclease-free water was injected in each dorsal blastomere of a 4-cell stage *Xenopus*
350 embryo. Injections were performed as previously described[32].

351 Embryos were grown at 14-16°C with daily cleaning in 0.1X Modified Barth's Saline (10X MBS:
352 88mM NaCL, 2.4mM NaHCO3, 1mM HEPES, 0.82mM MgSO4, 0.33mM Ca(NO3)2, 0.41 mM
353 CaCl2, pH 7.6).

354 All dissections took place at stage 35/36 (stages according to Nieuwkoop and Faber[33]). In the
355 case of dextran-injected embryos, embryos were screened using a fluorescence
356 stereomicroscope prior to dissection to ensure the presence of dextran in the eye primordia
357 (note that dextran-injected embryos are morphologically normal). Embryos were anesthetized
358 prior to dissection in 20% tricaine methanesulfonate solution (MS222, pH 7.6-7.8, with 1x PSF)
359 and subsequently immobilized in a Sylgard®184-lined petri dish using a bent 0.2 mm insect bin
360 (Austerlitz). Eye primordia were carefully explanted using a 0.15 mm insect pin (Austerlitz) held
361 in a pin holder. Explants were immediately transferred to 60% L15 media (Sigma-Aldrich, L4386,
362 pH 7.6-7.8, with 1x PSF, henceforth referred to as 'Xenopus culture media').

363 Following dissection, explants were placed with the lens facing up onto PAA gels or glass bottom
364 culture dishes. The hydrogels were prepared as described below.

365 Hydrogels and glass dishes were coated overnight (hydrogels) or for 30 min (glass) with 0.01
366 mg/ml PDL (Sigma-Aldrich, P6407, diluted in PBS) followed by 2 h in 5 µg/mL laminin (Sigma-
367 Aldrich, L2020, diluted in PBS). Following explant plating, dishes were allowed to sit for 1-2 h on
368 the benchtop to allow explants to adhere, and then were moved to a 20°C incubator overnight.

369 Immunostainings

370 Cells were washed twice with prewarmed (37°C) PBS. Afterwards, they were fixed and
371 permeabilized with 4% PFA (Thermo Fisher 28908) and 0.2% tritonX (Sigma-Aldrich T8787) in PBS
372 for 10 min at room temperature (RT). The cells were washed once with PBS at RT. Cells were
373 incubated with DAPI (1.7 µg/ml Sigma-Aldrich D9542) and Phalloidin (Life Technologies A12379,
374 diluted 1:300) in 1% Bovine Serum Albumin (Sigma-Aldrich A3294) in PBS for 1 h at RT. In the
375 end, the dishes were washed twice with PBS. Cells were imaged with a Leica DMi8
376 epifluorescence setup with a ×63 oil objective (NA 1.4, Leica).

377 Optical tweezers and force measurement

378 OT measurements took place on a custom-built inverted microscope[34]. Briefly, a 5 W 1064 nm
379 ytterbium fibre laser (YLM-5-LP, IPG Laser, Germany) was used at a high power (> 1 W) to
380 minimize intensity fluctuations. Excess power was redirected to a beam dump and the power at
381 the optical trap itself was 600 mW. The trap was generated by overfilling the back aperture of an
382 NA 1.2 UPlanSApo water immersion objective (Olympus, Japan) with the laser beam.

383 To enable controlled positioning of samples, the sample stage was mounted on top of a precision
384 piezoelectric stage (P-517.43 and E-710.3, Physik Instrumente, Germany) with a positioning
385 resolution of 1 nm. The sample stage was illuminated by a white fibre light source (DC-950 Fiber-
386 Lite, Edmund Optics, USA). White light entered the objective and then passed through a dichroic
387 mirror (DM) to a 550 nm short pass DM (DMSP550, Thorlabs, USA). This passed light below 550
388 nm to the 532 nm notch DM. This mirror coupled the fluorescence laser into the microscope,
389 and in the process blocked the portion of incoming white light ranging from 515 to 540 nm. Light
390 that passed through the notch DM was focused onto a CMOS camera (MC1362, Mikrotron,
391 Germany), which was used for tracking particles in the optical trap. Light above 550 nm was
392 passed to the fluorescence imaging camera (optiMOS Scientific CMOS, Teledyne Imaging, USA),
393 which was used to find beads to trap, locate cells, and record fluorescence images of tethers.

394 Forces were measured with the OT by modelling a particle in the trap potential as a Hookean
395 mass and spring system. By tracking the position of a trapped particle and multiplying this by a
396 calibrated trap stiffness constant, the force experienced by the particle was determined. Trap
397 calibration was performed using the power spectrum method[35]. Postprocessing of the data was
398 done using a custom script in Python 3.6, which is available on GitHub
399 https://github.com/mchughj33/mem-tension.

400 **OT bead functionalisation**

401 As reported previously[36,37], beads with 2 µm diameter (Kisker PC-S-2.0) were functionalized with
402 Concanavalin A (ConA, from Canavalia, Sigma-Aldrich, C2272-10MG) as follows.

403 10 µL bead solution were added into 100 µL of 2 mg/mL ConA in a tube (low-protein binding)
404 and incubated for 30 min at 4°C. Beads were washed twice via centrifugation in 100µL of
405 5mg/mL bovine serum albumin (BSA, Sigma-Aldrich, A3294) in 200mM Tris (Sigma, GE17-1321-
406 01) in ddH2O. All centrifugation steps were conducted at 4°C, 10,000 rcf. After the final wash, 1
407 ml imaging media supplemented with 1% PSF was added and gently mixed by pipetting.

408 **Membrane tether pulling experiments**

409 15 min prior to each fibroblast measurement, the culture media was exchanged with prewarmed
410 (37°C) imaging media supplemented with 1% PSF. For Xenopus experiments, Xenopus media was
411 exchanged with RT imaging media ~15 minutes prior to imaging.

412 In each OT experiment, 2 µl functionalised beads (see above) were added to the culture media
413 and a bead captured in the trap. During the entire process, the position of the bead relative to
414 the laser trap was recorded in order to measure the force produced by the tether pull. Before
415 attaching the bead to the cell, a short recording of the Brownian motion of the trapped bead was
416 taken. The mean force from each recording was used to define the point of zero force in the
417 subsequent analysis of each respective pull. Afterwards, the bead was carefully brought into
418 contact with the cell membrane. The image of the bead was monitored for a change in the
419 interference pattern around the bead, indicating contact between the bead and membrane. At
420 this point the beads was held stationary for 5 s. Then it was moved approximately 0.25 µm away
421 from the cell while monitoring the particle tracking system to see if the mean displacement of
422 the bead from the trap centre was reduced, which signified that the bead was attached to the
423 membrane.

424 Beads were then moved away from the cell at 0.1 µm s^{-1} in the case of 3T3 fibroblasts and 0.5
425 µm s^{-1} in the case of neurons, leading to the formation of a membrane tether between the cell
426 and the bead. After reaching the end of the pull, 10 µm for 3T3 fibroblasts and 20 µm for
427 neurons, the bead was held stationary for 30 s. The protocol for pulling tethers from neurons
428 was based on previous work[38]. Due to high rate of tether loss during preliminary pulls with
429 fibroblasts, to the pulling velocity was reduced, leading to a subsequent decrease in the pull
430 distance to avoid reducing experimental throughput. Pontes et al. showed that varying the
431 velocities for tether pulls in 3T3 fibroblasts within the range of 0.07 µm/s to 1µm/s, did not
432 affect the force results[39]. We therefore do not expect this velocity change to affect our
433 observations. For each pull, the peak force was defined as the maximum force value reached,
434 and the steady state force was determined as the mean of the 30 s period at the end of the pull
435 during which the bead was held stationary. Analysis was performed using custom analysis scripts
436 written in python 3.6.

437 Hydrogels for fibroblasts

438 Deformable hydroxy-polyacryamide substrates for fibroblast cultures were prepared as
439 described previously[22,40]. Briefly, for each gel a top coverslip and a glass-bottomed culture dishe
440 (MatTek P35G-0.20-C and Ibidi 81158 were used for OT and TFM, respectively) were prepared.
441 Both coverslips were first washed in 70% ethanol and distilled water, and then dried. Bottom
442 coverslips were wiped with a cotton bud soaked in 1M NaOH, dried, and then incubated in (3-
443 aminopropyl)trimethoxysilane (APTMS, Sigma Aldrich, 281778) for 3 min. APTMS was washed off
444 thoroughly in ddH20 and coverslips were then incubated in a 0.5% solution of glutaraldehyde
445 (Sigma Aldrich, G6257) for 30 min and then rinsed 3x with distilled water. Top coverslips were

446 treated for 10 min with Rain-X (Shell Car Care International). Acrylamide (AA, Sigma Aldrich,
447 A4058) stock solution was made by mixing 500 µL of 40% Acrylamide + 65 µL of 100%
448 Hydroxyacrylamide (Sigma Aldrich, 697931). Afterwards the gel premix was prepared by mixing
449 500 µL Acrylamide stock solution with 250 µL 2% Bisacrylamide (BA, Fisher Scientific, BP1404-
450 250). The premix was diluted in PBS to achieve the different shear moduli according to the **table**
451 **1.** For TFM gels, 10 µL of PBS was replaced by 10 µl bead solution (FluoSpheres™ Carboxylate-
452 Modified Microspheres, 0.2 µm, dark red fluorescent)) and the gel mix was sonicated for 30 s to
453 separate the beads.

Volume of gel premix	Volume of PBS	Shear modulus (G')
53 µL	447 µL	0.1 kPa
75 µL	425 µL	1 kPa
150 µL	350 µL	10 kPa

454 **Table 1: Hydroxy-polyacrylamide gel composition used for fibroblasts**
455
456 Freshly-made premixes were de-gassed under vacuum for 4-6 min. To each 500 µL of final gel
457 solution, 1.5 µL 0.3% (v/v) N, N, N', N'-tetramethylethylenediamine (TEMED, Thermo Fisher,
458 15524–010) and 5 µL 0.1% (w/v) ammonium persulfate (APS, Sigma, 215589) solution were
459 added and the premix was gently mixed. 14 µL or 10 µL of this mixture were pipetted on the
460 bottom coverslip and 18 mm or 16 mm top coverslips (for 14 µL and 10 µL volume, respectively)
461 were placed on top (with RainX-treated side facing down). The gels were soaked in PBS for at

462 least 20 min before the top coverslips were removed. Afterwards, they were washed twice with
463 PBS and then treated with ultraviolet light for 30 min. Hydrogels were coated as described
464 above.

465 Hydrogels for neurons

466 Deformable polyacrylamide gel substrates were prepared as described previously[41,42] for neuron
467 culture. The coverslips were prepared as described in the hydroxy-acryamide gel protocol using
468 MatTek dishes as the bottom coverslip. The gel mix was prepared according to **table 2** to achieve
469 the different shear moduli. For TFM gels, the PBS volume was reduced by 10 µL and replaced by
470 10 µL bead solution and the gel mix was sonicated for 30 s to separate the beads.

Volume of AA	Volume of BA	Volume of PBS	Shear modulus (G')
63 µL	10 µL	427 µL	0.1 kPa
63 µL	17.5 µL	419.5 µL	0.3 kPa
94 µL	15 µL	391 µL	1 kPa

471
472 Table 2: Polyacryamide gel composition used for neurons
473

474 Freshly-made gel mixes were briefly de-gassed under vacuum for 4-6 min. To each 500 µL of final
475 gel solution, 1.5 µL 0.3% (v/v) TEMED and 5 µL 0.1% (w/v) APS solution were added and gently
476 mixed. 7 µL, 14 µL of this mixture were pipetted onto the bottom coverslip and 18 mm top
477 coverslips were placed on top (with RainX treated side facing down) for OT experiments and TFM

478 experiments, respectively. The gels were soaked in PBS for at least 20 min before the top
479 coverslips were removed. The gels were subsequently functionalized via a 4h treatment with
480 hydrazine hydrate (Sigma Aldrich, 225819), followed by 1 h in 5% acetic acid (Fisher Scientific,
481 10171460), and then washed thoroughly in PBS. Afterwards, they were treated with ultraviolet
482 light for 30 min. Hydrogels were coated as described above.

483 TFM

484 24 h after plating, fibroblasts were imaged with an inverted microscope (Leica DMi8) at 37°C and
485 5% CO_2, equipped with a digital sCMOS camera (ORCA-Flash4.0, Hamamatsu Photonics), an
486 EL6000 illuminator (Leica) and a ×63 oil objective (NA = 1.4, Leica). Images were acquired with
487 Leica LAS X software. Fluorescence images of beads and wide-field images of cells were taken
488 every 2 min for 10 minutes. After image acquisition, the culture media was exchanged with
489 Trypsin-EDTA (Gibco) to detach cells from the gel. Reference images of fluorescent beads were
490 taken 15 min after trypsinization.

491 16 - 24 h after plating, *Xenopus* eye primordia explants were imaged using an inverted Nikon
492 microscope (Ti-E at room temperature) equipped with an sCMOS camera (Prime BSI Scientific,
493 Photometrics), a CoolLED pE-4000, and ×60 oil objective (NA = 1.4, Nikon). Fluorescence images
494 of beads and wide-field images of cells were taken every 5 min for 1 h. After image acquisition,
495 the culture media was exchanged with Trypsin-EDTA (Gibco) or 20% sodium dodecyl sulfate
496 solution (Severn Biotech Ltd., 2 0-4002-01) to detach the explants from the gel. Reference
497 images of fluorescent beads were taken 15 min after trypsinization or immediately after sodium
498 dodecyl sulfate treatment.

499 Traction stress maps were calculated for each frame. Traction stresses were averaged over time
500 (12 frames for neurons*, 5* frames for fibroblasts) for each cell. Postprocessing of the data and
501 statistical analyses were done with a custom script in Python 3.8 and is available on GitHub
502 https://github.com/rg314/pytraction.

503 **Statistics**

504 OT data are shown as violin plots, TFM data as box plots. Violin shapes are kernel density
505 estimations, boxes indicate the range of data that falls between the first and third quartile,
506 whiskers show the range of data within 1.5 times the interquartile range. Density estimator
507 width is based on the number of samples at a given value. Median values for each dataset are
508 marked by a white circle. Lines between violins indicate significant differences in the samples.
509 The boxplot diagrams were generated using python seaborn. The borders of the box indicate the
510 quartiles of the dataset, the median is indicated by a line within the box, and the whiskers
511 include 1.5*interquartile range. Points that were determined to be outliers were plotted
512 individually. Kruskal-Wallis one-way analysis of variance (ANOVA) tests followed by a Tukey
513 posthoc test were used for statistical analysis when comparing multiple groups. When
514 comparing two groups, a Mann-Whitney test was used.